Article

Photophysical Characteristics of Multicolor Emitting MDMO-PPV–DMP/ZnO Hybrid Nanocomposites

Bandar Ali Al-Asbahi * , **Arwa Alhamedi Alanezi** and **Mohamad S. AlSalhi**

Department of Physics & Astronomy, College of Sciences, King Saud University, P.O. Box 2455, Riyadh 11451, Saudi Arabia; 439203076@student.ksu.edu.sa (A.A.A.); malsalhi@ksu.edu.sa (M.S.A.)
* Correspondence: balasbahi@ksu.edu.sa

Abstract: The tuning of photophysical properties of the poly[2-methoxy-5-(3,7-dimethyl-octyloxy)-1,4-phenylenevinylene]—end capped with dimethylphenyl (DMP), MDMO-PPV–DMP, was achieved by incorporation of ZnO NPs with various contents. Hybrid nanocomposites of MDMO-PPV–DMP with ZnO NPs were prepared by solution blending method and then deposited onto glass substrates. The structural properties of the hybrid nanocomposites samples were characterized using X-ray diffraction, FTIR, and FE-SEM, while their optical properties were extracted from the absorption and photoluminescence spectra. The energy band gap, energy tail, steepness parameter, and CIE chromatic coordinates were tuned by increase the content of ZnO NPs into the polymer matrix. The ZnO NPs incorporation assists the emission wavelength shift and multicolor emitting from the hybrid nanocomposites.

Keywords: hybrid nanocomposite; photophysical properties; MDMO-PPV–DMP; ZnO NPs

1. Introduction

Numerous types of electroluminescent and conducting polymers have been specified as a promising kind of materials for optoelectronic applications such as organic light emitting diodes (OLEDs), organic photovoltaic cells, organic phototransistors, and organic photo detectors. New research based on the conductive polymers has been opened up to improve a new technology of plastic electronics. When the conducting polymers are forward biased by direct current, they emit light via holes–electrons recombination. The energy difference between the lowest unoccupied molecular orbit (LUMO) level and highest occupied molecular orbit (HOMO) level will play a crucial role in determining the light color (emitted photon wavelength).

The manufacture of the optoelectronic devices based on derivatives of poly (p-phenylene vinylene) (PPV) has attracted the interest of researchers. In particular, poly[2-methoxy-5-(3,7-dimethyl-octyloxy)-1,4-phenylenevinylene], MDMO-PPV, is one of the most broadly considered of these derivatives because of its high stability, unique electroluminescent properties, and particular structure that allow easy deposition in flexible circuits, large-area electronics, and low-cost printable electronics [1–4]. Moreover, MDMO-PPV is an electron donating material and has acquired historical importance as the material for which electroluminescent in conjugated polymers was discovered in 1990 [5].

According to numerous studies it was found that the OLED devices based on polymers inherit two major problems, namely, poor optical absorption and lack of carrier mobilities [6]. To overcome the major problems of the OLEDs and thus improve their performance, the inorganic nanostructures were incorporated into the polymer [7,8]. Numerous studies have been reported on optoelectronic devices based on nanocomposite of polymer and metal oxide nanoparticles. It was found that the nanocomposites improve the stability and the optoelectronic properties of the organic devices. Despite this, the optical and structural properties of the polymer are still a topic of investigation. Baraton and co-workers reported

that the conjugation lengths of PPV do not break upon inclusion of TiO2 NPs [9]. However, Yang and co-workers observed that the PPV conjugation length was gradually reduced with increments of the SiO_2 NPs [10].

In this paper, ZnO NPs successfully dispersed into the poly[2-methoxy-5-(3,7-dimethyl-octyloxy)-1,4-phenylenevinylene]—end capped with dimethylphenyl (MDMO-PPV–DMP) for better photophysical properties and tuning of color emission. ZnO NPs is an n-type semiconducting material with a wide bandgap, high exiton binding energy, high optical transparency, and is nontoxic. MDMO-PPV is p-type polymer, light-emitting polymer, soluble in common organic solvents, and widely used in photovoltage devices. Thus, tailoring the property of both ZnO and polymer, and creating a nanocomposite hybrid with enhanced properties can be achieved by incorporation of ZnO NPs with emitting polymers. For this purpose, the influence of the incorporation of various weight percentages of ZnO NPs on the photophysical properties of the MDMO-PPV–DMP/ZnO hybrid nanocomposite will be explained in detail.

2. Results and Discussion

The X-ray diffractograms of the thin films of pristine MDMO-PPV–DMP, and MZNCs are shown in Figure 1. The broad band in the 2θ range of 15–30° confirms the amorphous phase of the pristine MDMO-PPV–DMP. The sample's crystallinity was slightly enhanced upon incorporation of the ZnO NPs as evidenced from the narrowing the broad band of the MDMO-PPV–DMP. The broad band became clearer and less broadening with the increase of the ZnO NPs content, confirming the incorporation of ZnO NPs into the MDMO-PPV–DMP matrix and the nanocomposite structure formation [11]. Moreover, the broad band of MDMO-PPV–DMP was hardly observed in the diffractograms of the hybrid 50MZNCs due to lower scattering factors compared to ZnO NPs.
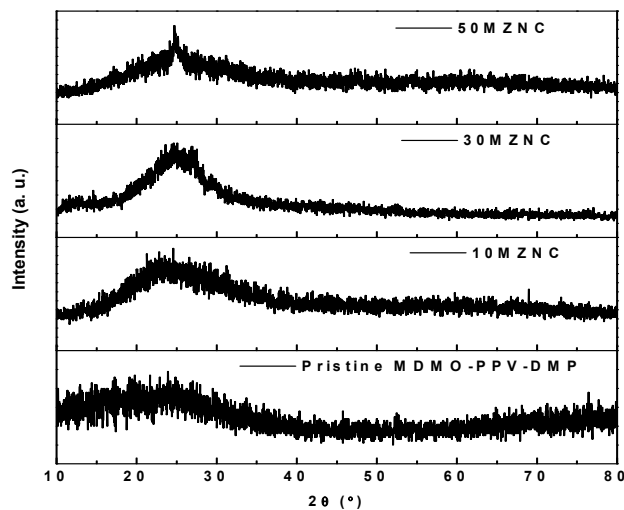

Figure 1. XRD diffractograms of pristine MDMO-PPV–DMP and MZNCs thin films.

The nature of the chemical groups of pristine MDMO-PPV–DMP and the hybrids of MZNCs can be seen in the FTIR spectra in Figure 2. Many bands in the range of 4000–400 cm^{-1} were revealed for all samples. The transmission peaks at 3061 and 3450 cm^{-1} assigned to C-H stretching in the benzene ring and O-H stretching, respectively, whereas the vibrational modes at 2926 cm^{-1}, 2951 cm^{-1}, and 2860 cm^{-1} denote the asymmetrical and symmetrical CH_2 and CH_3 stretching. The preparation of the samples disks in an open-air atmosphere resulted in formation band at 1633 cm^{-1} due to H-O-H bending vibration mode [12]. Two semicircular stretch modes can be assigned to the phenyl ring at 1506 and 1413 cm^{-1} [13]. The bands at 1472 and 1354 cm^{-1} refer to antisymmetric and symmetric alkyl CH_2, respectively. The peaks at 1252, 1202, and 1040 cm^{-1} are associated with C-O stretching in ether groups, phenyl oxygen stretch, and alkyl oxygen

stretch, respectively [11,14]. The bands at 957 cm^{-1} and 855 cm^{-1} are associating with trans double bond vinylene C-H wagging and phenyl C-H wagging, respectively, which indicates the dipole normal to the phenyl vinyl plane [15]. A new band at 1092 cm^{-1} was detected in the transmission spectra of MZNCs with a gradual increase up to 1126 cm^{-1} upon incorporation of ZnO NPs. This shifting in the new band can be attributed to the deprotonating that signifies the transfer or removal of protons (H$^+$ ions) due to O^{2-} in ZnO and thus induces stress in the C-H bonding [16].
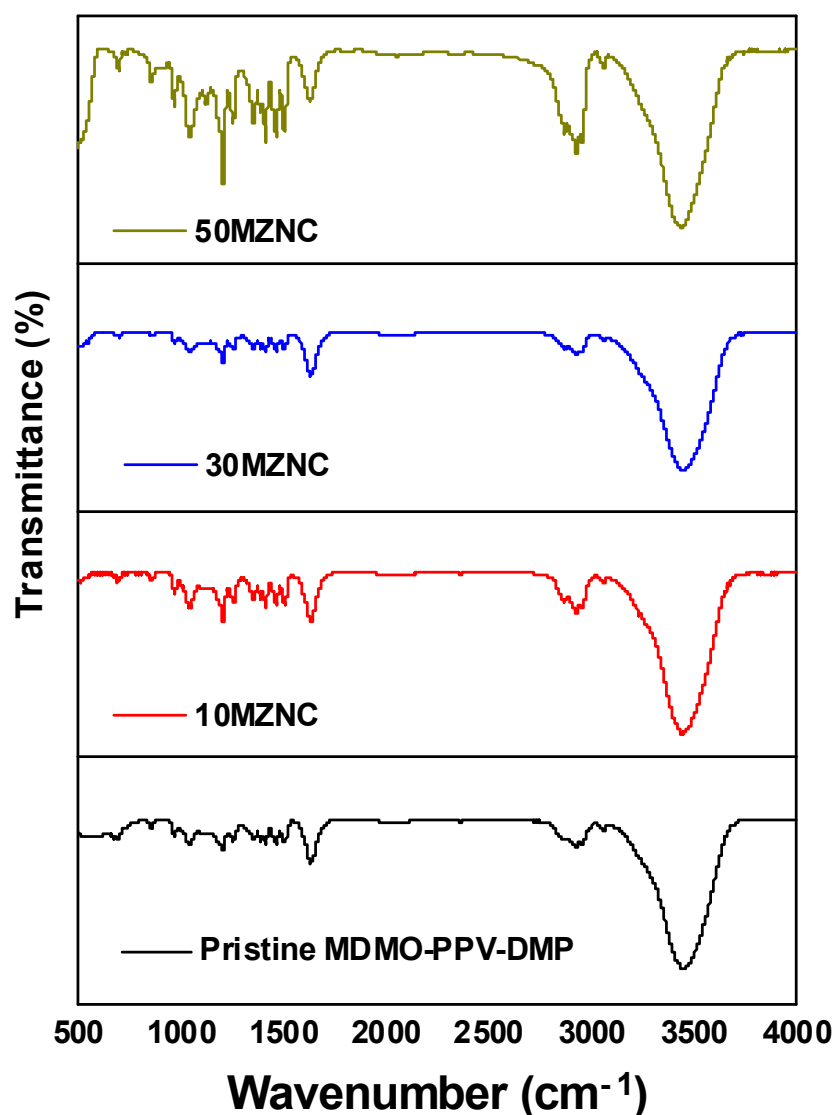

Figure 2. FTIR spectra of pristine MDMO-PPV–DMP and the MZNCs thin films.

Figure 3 displayed the surface morphology of MZNCs thin films under scales 100 nm and 1μm. The distribution of the ZnO NPs on the MDMO-PPV–DMP matrix can be clearly observed. The images with a scale of 100 nm confirmed the uniform particle shape of the ZnO NPs, while the homogeneous distribution of the nanoparticles on the matrix thin film with presence agglomeration at the high content of ZnO NPs (≥30 wt.%) was observed from the images with a scale of 1μm. This agglomeration with inclusion of ZnO NPs in the MDMO-PPV–DMP matrix plays crucial role to enhance the conformational disorder [17–19].

The absorption spectra of all thin films of pristine MDMO-PPV–DMP and MZNCs were demonstrated in Figure 4. Two main absorption peaks were detected for pristine MDMO-PPV–DMP at 342 and 492 nm, corresponding to 0–1 and 0–0 vibronic transitions,

respectively. The increase of the absorbance can be ascribed to scattering caused by the ZnO NPs in the MDMO-PPV–DMP matrix, which is expected to rise in increments with the ZnO NPs content. The main absorbance peak at 492 was slightly red shifted with increments with the ZnO NPs content and reached to 499 nm for 40MZNC. This result may lead to the possibility of extending conjugation length of the MDMO-PPV–DMP when the ZnO NPs content is increased [20]. The non-uniform change in the absorbance with the ZnO NPs content is due to the change in the homogeneous distribution quality with increments with the ZnO NPs content. At a low content of ZnO NPs (5 and 10 wt.%), the absorbance decreased due to good distribution into the polymer matrix and then dramatically increased with increments with the ZnO NPs content (20–40 wt.%). This rise in absorbance could be justified in terms of increasing the aggregation with increasing ZnO NPs content. This is unlike the behavior which occurred with 50MZNC, where the absorption became nearly constant for the entire wavelength range, indicating aggregation of the MDMO-PPV–DMP chain or as a result of the relatively long conjugated chains. Similar behavior was observed with another system of MEH-PPV/CdTe nanocomposite at a high content of the CdTe nanoparticles [21].
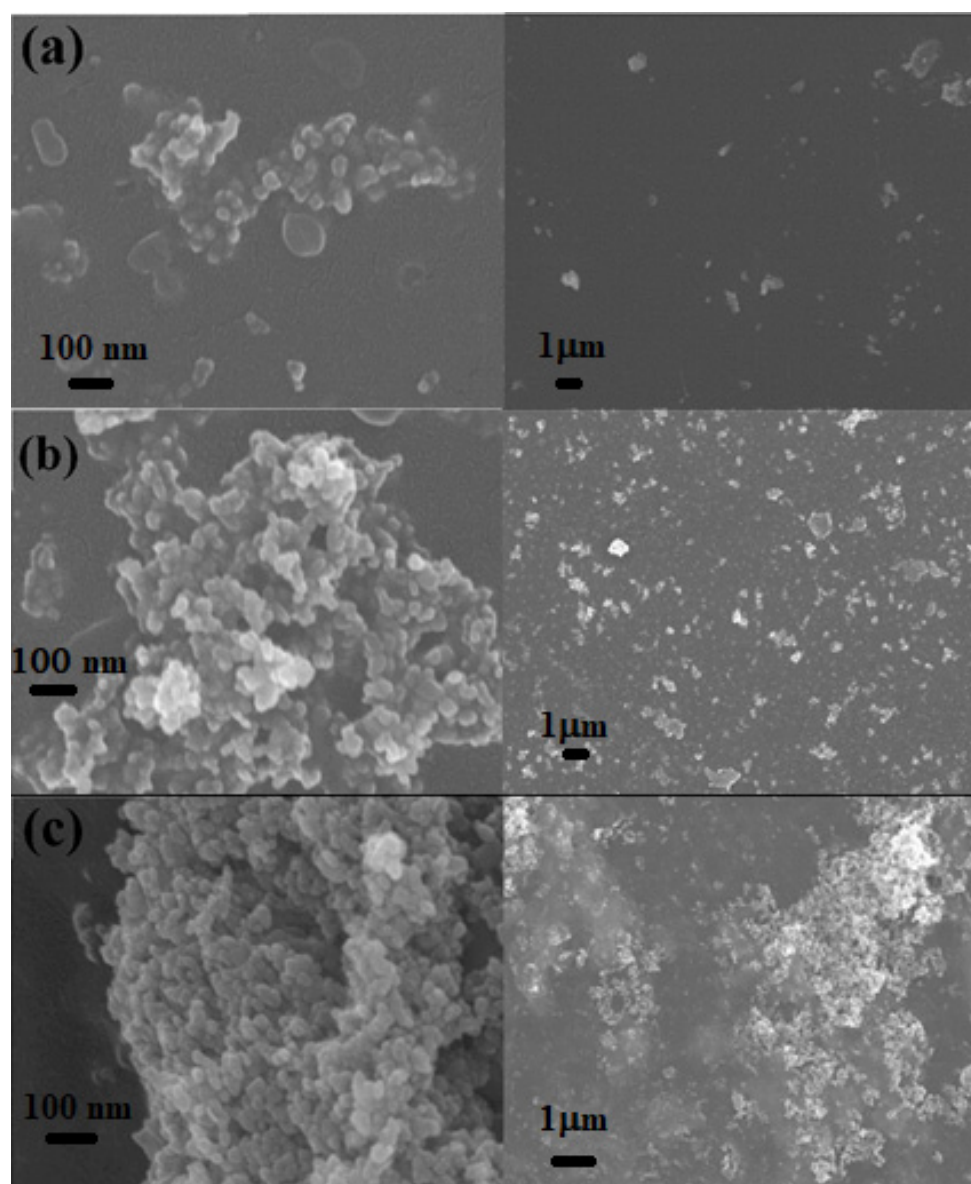

Figure 3. FE-SEM images of (**a**) 10MZNC, (**b**) 30MZNC, and (**c**) 50MZNC thin films under scales of 100 nm and 1μm for each thin film.
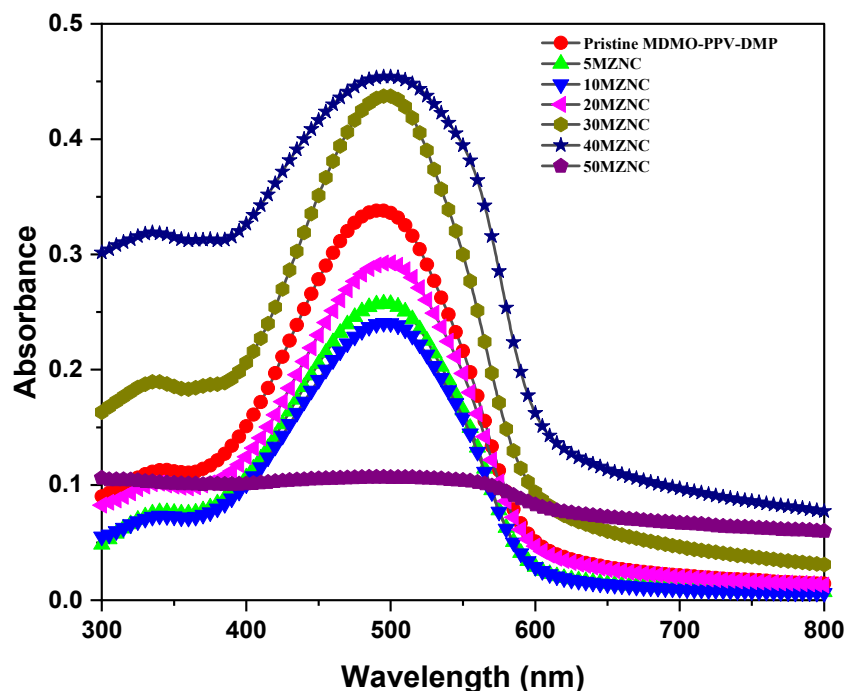
Figure 4. Absorption spectra of pristine MDMO-PPV–DMP and the MZNCs thin films.

The influence of the ZnO NPs content on the values of direct and indirect energy band gap (E_{gd} and E_{gi}) of the MDMO-PPV–DMP thin film could be estimated by the extrapolating method using the $(\alpha h\nu)^2$ and $(\alpha h\nu)^{1/2}$ versus photon energy ($h\nu$) plot, respectively, as presented in Figure 5, where α is the absorption coefficient. The values of E_{gd} and E_{gi} can be obtained by extrapolation of the linear portion of each curve in Figure 5, and then listed in Table 1. The E_{gd} and E_{gi} values of MDMO-PPV–DMP thin film were found to be 2.18 eV and 2.06 eV, respectively. These obtained band gaps of MDMO-PPV–DMP are in agreement with previous reports [22,23]. These values of both E_{gd} and E_{gi} were dramatically reduced upon increment of ZnO NPs to reach 2.03 eV and 1.89 eV, respectively. The reduction in the energy band gap of the MDMO-PPV–DMP indicates that the conduction band and the valence band are getting closer to each other. The presence of both types of energy band gaps in MZNCs thin films can broaden the range of absorption energy to improve the photoelectric energy conversion [24]. Moreover, the close values of both E_{gd} and E_{gi} from each other make such that these hybrids are an effective material in optoelectronic devices.
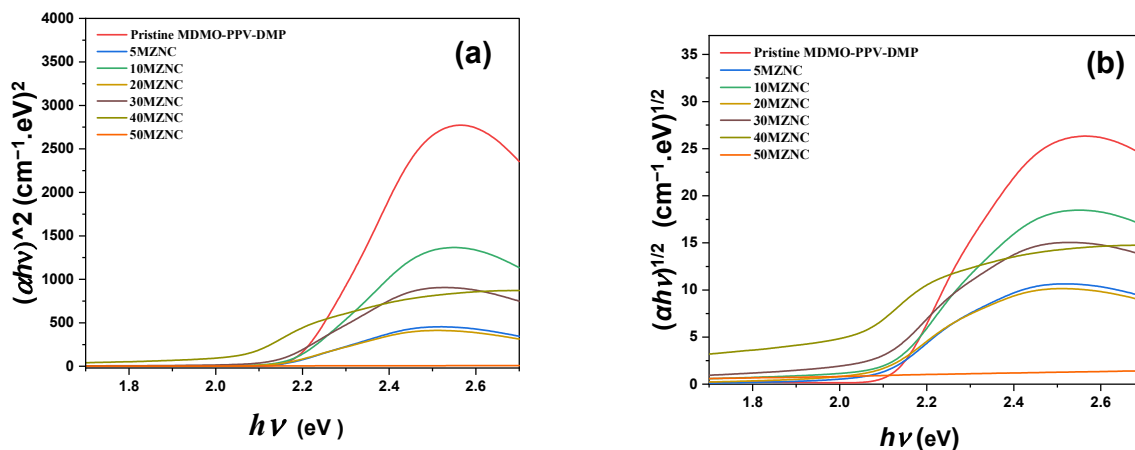

Figure 5. (**a**) plot of $(\alpha h\nu)^2$ vis. $h\nu$, and (**b**) $(\alpha h\nu)^{1/2}$ vis. $h\nu$ plot for pristine MDMO-PPV–DMP and the MZNCs thin films.

Table 1. Optical parameters of pristine MDMO-PPV–DMP and the MZNCs thin films.

Specimen	Egd (eV)	Egi (eV)	Eu (eV)	$\sigma = K_\beta T/E_u$
Pristine MDMO-PPV–DMP	2.18	2.06	0.0418	0.6143
5MZNC	2.14	2.05	0.0888	0.2892
10MZNC	2.16	2.01	0.0950	0.2705
20MZNC	2.14	2.03	0.1029	0.2496
30MZNC	2.11	2.04	0.1303	0.1971
40MZNC	2.03	1.89	0.2238	0.1147
50MZNC	-	-	0.2012	0.1277

The tail width of localized states in the forbidden band gap can be reflected by energy gap tail (E_u), which is less than the band gap energy. The Urbach plots for all thin films are displayed in Figure 6. The E_u values were estimated from the inverse slope of the linear part of the Urbach plots [25], as seen in Table 1. The higher incorporation of the ZnO NPs into the MDMO-PPV–DMP resulted in a systematic increase in the E_u values and thus formation of imperfections and disorder in the band structure of the nanocomposites in addition to the creation of more localized states within the forbidden gap [26,27]. The shrinkage/widening of the optical absorption edge can be described by the steepness parameter ($\sigma = K_\beta T/E_u$), where T and k_β are the absolute temperature and the Boltzmann constant, respectively. As demonstrated in Table 1, the σ value was decreased with increment of the ZnO NPs. This decrease can be ascribed to the rise in the localized density of electronic states within the forbidden band gap of the hybrid nanocomposites [18,28].
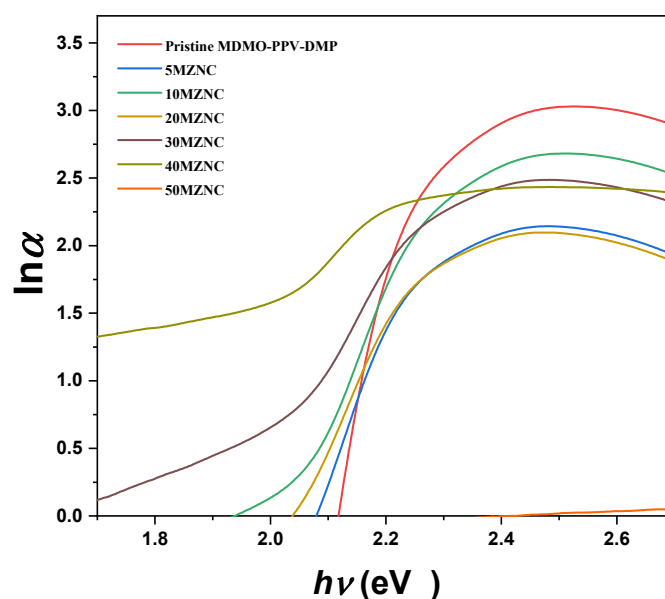
Figure 6. Urbach plots of pristine MDMO-PPV–DMP and the MZNCs thin films.

The photoluminescence (PL) spectra were recorded in Figure 7 to study the behavior of the molecules in the excited state in the absence and presence of the ZnO NPs with various ratios. The PL spectra were collected for wavelengths in the range of 500 to 700 nm with the excitation wavelength fixed at 480 nm. At low content of ZnO NPs (5 and 10 wt.%), no significant change was observed. At higher content, significant changes in both PL intensity and shifting of the PL peak were detected. The emission intensity of the MDMO-PPV–DMP with the main peak at 575 nm was systematically enhanced upon increment the ZnO NPs and red shifted to reach 592 nm at 50 wt.%. The improvement in the intensity can be interpreted to chain separation and/or the charge trapping effect [18,29]. As ZnO is an n-type semiconductor with a stronger electron affinity, more holes can be allowed to recombine through the MDMO-PPV–DMP/ZnO interface and thus enhance the emission

intensities [30]. The maximum emission was detected for 40MZNC. The quenching in the emission intensity by incorporation more ZnO NPs (50 wt.%) can be attributed to that the higher aggregation resulted in plenty of electrons which were mostly blocked around the ZnO surface and confined the recombination population for the nanocomposite hybrid of MDMO-PPV–DMP/ZnO. Similar behavior was observed with other systems such as PFO-oxe/ZnO [29]. On the other hand, the red shift in the PL spectrum is associated with changes in the conjugation length [31]. The inclusion of the ZnO NPs in the MDMO-PPV–DMP matrix leads to separation in the polymer chains and thus changes in the conjugation length of the polymer resulting in a red shift in the PL spectra. Moreover, a new peak at 663 nm can be noted at high content of ZnO NPs (≥20 wt.%), which can be attributed to intrachain electronic states [32].
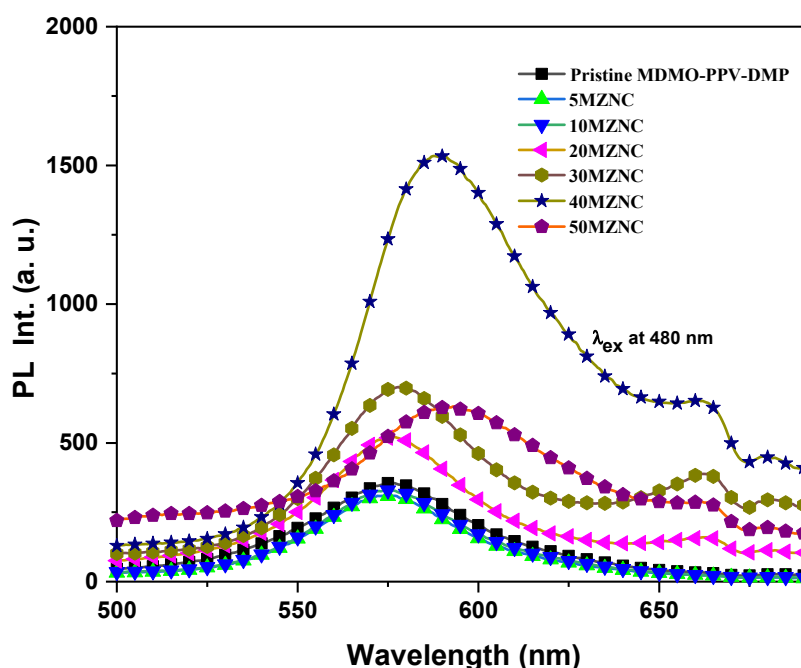

Figure 7. PL spectra of pristine MDMO-PPV–DMP and the MZNCs thin films.

Figure 8a shows the CIE chromaticity diagram which identifies the perceived color of the emission spectrum of pristine MDMO-PPV–DMP and the MZNCs thin films. The CIE 1931 chromaticity diagrammed in Figure 8b was used as a reference [33,34] to characterize the color emission generated from each thin film that was excited at 480 nm. The (x, y) coordinates corresponding to all thin films are presented in Table 2. As the ZnO NPs contents are increased, the (x, y) coordinates are turned from the greenish yellow region to the white region on the chromaticity diagram. It can be concluded that the new peak that is created in the PL spectra (Figure 7) at ≥20 wt.% of ZnO NPs played a crucial role to produce the white emission.

Table 2. Experimental CIE coordinates corresponding of pristine MDMO-PPV–DMP and the MZNCs thin films.

Specimen	X	Y	Color
Pristine MDMO-PPV-DMP	0.4238	0.4446	Greenish yellow
5MZNC	0.4167	0.4283	Greenish yellow
10MZNC	0.4221	0.4316	Greenish yellow
20MZNC	0.4126	0.3980	white
30MZNC	0.4083	0.3501	white
40MZNC	0.4838	0.3700	Orange pink
50MZNC	0.4165	0.3724	white

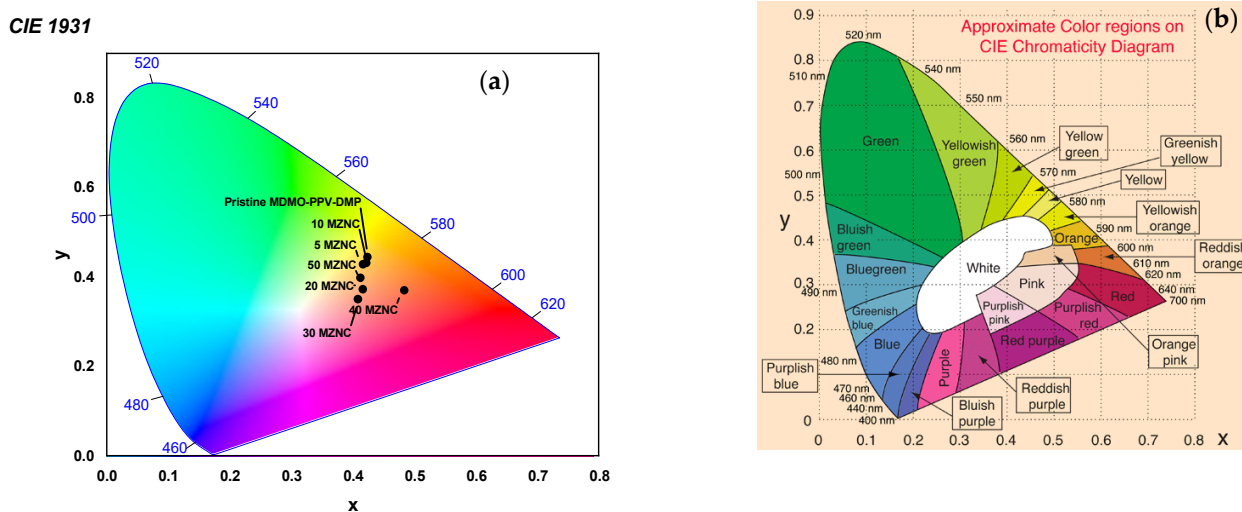**Figure 8.** (**a**) (x, y) chromaticity coordinates generated from pristine MDMO-PPV–DMP and the MZNCs thin films, (**b**) CIE 1931 color space chromaticity diagram.

3. Materials and Methods

MDMO-PPV–DMP, with a molecular weight of 100,000 g/mol was purchased from American Dye Source, Inc. (Morgan Boulevard, QC, Canada), and ZnO NPs with a mean size of ~25 nm in wurtzite phase, was purchased from Sigma-Aldrich (St. Louis, MO, USA).

The nanoparticles of ZnO were dispersed into ethanol with 2 vol.% of Ethylene Glycol, stirred at 600 rpm for 2 h, and sonicated for 1 h to obtain a homogeneous solution. By the solution blending method, ZnO NPs with different ratios (5, 10, 20, 30, 40, and 50 wt.%) were incorporated into a fixed toluene solution of MDMO-PPV–DMP (5 mg/mL). The hybrid of MDMO-PPV–DMP with 5, 10, 20, 30, 40, and 50 wt.% of ZnO NPs were labeled as 5MZNC, 10MZNC, 20MZNC, 30MZNC, 40MZNC, and 50MZNC, respectively. Fifty milliliters of each solution of pristine MDMO-PPV–DMP and MZNCs were deposited into cleaned glass substrates by spin coating technique (2000 rpm, 30 s) to prepare homogeneous thin films. All the thin films were dried at 120 °C for 10 min at ambient conditions prior to carry out all measurements.

X-ray diffraction (XRD; Miniflex 600, Rigaku, Latvija, Japan), Fourier transform infrared spectroscopy (FT-IR; PerkinElmer Spectrum 100, Waltham, MA, USA), and field emission scanning electron microscope (FE-SEM; JEOL JSM-7610F Tokyo, Japan) were utilized to characterize the structural properties of the hybrid nanocomposites. The optical properties of the samples were investigated by UV–vis Spectrophotometer (JASCO V-670, Cremella, Italia) and spectrofluorometer (JASCO FP-8200, Cremella, Italia). Moreover, the OriginLab program version 2019b (Northampton, MA, USA) was employed to obtain the CIE coordinates of all thin films from their emission spectra.

4. Conclusions

The incorporation of ZnO NPs with various content was successfully effective on both the optical and structure properties of MDMO-PPV-DMP. The crystallinity of the samples was slightly enhanced upon incorporation of the ZnO NPs. The homogeneous distribution of the ZnO NPs on the MDMO-PPV–DMP matrix was confirmed by FE-SEM images. The conjugation length of the MDMO-PPV–DMP was extended when the ZnO NPs content was increased. Both direct and indirect types of energy band gaps were found in MZNCs thin films and dramatically reduced upon increment of the ZnO NPs content. The formation of imperfections and disorder in the band structure of the nanocomposites in addition to the creation more localized states within the forbidden gap can be expected from a systematic increase in the Eu values and reduction in the s values upon incorporation of ZnO NPs into the MDMO-PPV–DMP. The inclusion of the ZnO NPs in the MDMO-PPV–DMP matrix

leads to enhancement of the PL intensity and tuning of the color emission. A new emission peak at 663 nm was noted at a high content of ZnO NPs ($\geq$20 wt.%), which can be attributed to intrachain electronic states, and played a crucial role to produce the white emission. The results obtained in this work confirm that the hybrid of MZNCs is an effective material if used in optoelectronic devices.

Author Contributions: Conceptualization, B.A.A.-A.; Data curation, B.A.A.-A. and A.A.A.; Formal analysis, B.A.A.-A. and A.A.A.; Funding acquisition, B.A.A.-A.; Investigation, B.A.A.-A., A.A.A. and M.S.A.; Methodology, B.A.A.-A. and A.A.A.; Project administration, B.A.A.-A.; Supervision, B.A.A.-A.; Validation, B.A.A.-A. and M.S.A.; Visualization, B.A.A.-A.; Writing—original draft, B.A.A.-A.; Writing—review and editing, B.A.A.-A. All authors have read and agreed to the published version of the manuscript.

References

1. Yang, S.-H.; Nguyen, T.; Le Rendu, P.; Hsu, C.-S. Optical and electrical properties of PPV/SiO$_2$ and PPV/TiO$_2$ composite materials. *Compos. Part A Appl. Sci.* **2005**, *36*, 509–513. [CrossRef]
2. Sekitani, T.; Yokota, T.; Zschieschang, U.; Klauk, H.; Bauer, S.; Takeuchi, K.; Takamiya, M.; Sakurai, T.; Someya, T. Organic nonvolatile memory transistors for flexible sensor arrays. *Science* **2009**, *326*, 1516–1519. [CrossRef] [PubMed]
3. Briseno, A.L.; Mannsfeld, S.C.; Ling, M.M.; Liu, S.; Tseng, R.J.; Reese, C.; Roberts, M.E.; Yang, Y.; Wudl, F.; Bao, Z. Patterning organic single-crystal transistor arrays. *Nature* **2006**, *444*, 913–917. [CrossRef]
4. Chua, L.-L.; Zaumseil, J.; Chang, J.-F.; Ou, E.C.-W.; Ho, P.K.-H.; Sirringhaus, H.; Friend, R.H. General observation of n-type field-effect behaviour in organic semiconductors. *Nature* **2005**, *434*, 194–199. [CrossRef] [PubMed]
5. Marks, R.; Mackay, K.; Friend, R.; Burnsf, P. Light-emitting diodes based on conjugated polymers. *Nature* **1990**, *6293*, 539–541.
6. Cui, Y.; Duan, X.; Hu, J.; Lieber, C.M.J. Doping and electrical transport in silicon nanowires. *Phys. Chem. B* **2000**, *104*, 5213–5216. [CrossRef]
7. Liu, J.; Qu, S.; Zeng, X.; Xu, Y.; Gou, X.; Wang, Z.; Zhou, H.; Wang, Z. Fabrication of ZnO and its enhancement of charge injection and transport in hybrid organic/inorganic light emitting devices. *Appl. Surf. Sci.* **2007**, *253*, 7506–7509. [CrossRef]
8. Quan, S.; Teng, F.; Xu, Z.; Wang, D.; Yang, S.; Hou, Y.; Wang, Y. Effect of inorganic nanolayers on electron injection in polymer light-emitting diodes. *Phys. Lett. A* **2006**, *352*, 434–437. [CrossRef]
9. Baraton, M.-I.; Merhari, L.; Wang, J.; Gonsalves, K.E. Investigation of the/PPV nanocomposite for gas sensing applications. *Nanotechnology* **1998**, *9*, 356. [CrossRef]
10. Yang, S.-H.; Nguyen, T.; Le Rendu, P.; Hsu, C.-S. Optical and electrical investigations of poly (p-phenylene vinylene)/silicon oxide and poly (p-phenylene vinylene)/titanium oxide nanocomposites. *Thin Solid Film.* **2005**, *471*, 230–235. [CrossRef]
11. Shankar, J.S.; Ashok Kumar, S.; Periyasamy, B.K.; Nayak, S.K. Studies on optical characteristics of multicolor emitting MEH-PPV/ZnO hybrid nanocomposite. *Polym. Plast. Technol. Mater.* **2019**, *58*, 148–157. [CrossRef]
12. Li, M.; Zhu, L.; Lin, D. Toxicity of ZnO nanoparticles to Escherichia coli: Mechanism and the influence of medium components. *Environ. Sci. Technol.* **2011**, *45*, 1977–1983. [CrossRef]
13. Madhugiri, S.; Dalton, A.; Gutierrez, J.; Ferraris, J.P.; Balkus, K.J.J. Electrospun MEH-PPV/SBA-15 composite nanofibers using a dual syringe method. *Am. Chem. Soc.* **2003**, *125*, 14531–14538. [CrossRef] [PubMed]
14. Li, Z.; Guan, H.; Yu, N.; Xu, Q.; Imae, I.; Wei, J.J. Conjugated Polymer Poly(2-methoxy-5-(3′,7′-dimethyloctyloxy)-1,4-phenylenevinylene) modification on carbon nanotubes with assistance of supercritical carbon dioxide: Chemical interaction, solubility, and light emission. *Phys. Chem. C* **2010**, *114*, 10119–10125. [CrossRef]
15. Juhari, N.; Majid, W.H.A.; Ibrahim, Z.A. Structural and optical studies of MEH-PPV using two different solvents prepared by spin coating technique. *Solid State Sci. Technol* **2007**, *15*, 141–146.
16. Sachdeva, H.; Saroj, R. ZnO nanoparticles as an efficient, heterogeneous, reusable, and ecofriendly catalyst for four-component one-pot green synthesis of pyranopyrazole derivatives in water. *Sci. World J.* **2013**, *2013*, 680671. [CrossRef]
17. Quan, S.; Teng, F.; Xu, Z.; Qian, L.; Hou, Y.; Wang, Y.; Xu, X. Solvent and concentration effects on fluorescence emission in MEH-PPV solution. *Eur. Polym. J.* **2006**, *42*, 228–233. [CrossRef]

18. Jumali, M.H.H.; Al-Asbahi, B.A.; Yap, C.C.; Salleh, M.M.; Alsalhi, M.S. Optoelectronic property enhancement of conjugated polymer in poly (9,9′-di-n-octylfluorenyl-2.7-diyl)/titania nanocomposites. *Thin Solid Films* **2012**, *524*, 257–262. [CrossRef]

19. Quan, S.; Teng, F.; Xu, Z.; Zhang, T.; Qian, L.; Liu, D.; Hou, Y.; Wang, Y. Temperature effects on photoluminescence of poly[2-methoxy-5-(20-ethyl-hexyloxy)-1, 4-phenylene vinylene]. *Mater. Lett.* **2006**, *60*, 1134–1136. [CrossRef]

20. Chen, G.; Wang, P.J. Alteration of the optical properties of poly 9, 9′-dioctylfluorene by TiO_2 nanocrystalline. *Non Cryst. Solids* **2006**, *352*, 2536–2538. [CrossRef]

21. Verma, D.; Rao, A.R.; Dutta, V. Surfactant-free CdTe nanoparticles mixed MEH-PPV hybrid solar cell deposited by spin coating technique. *Sol. Energy Mater Sol. Cells* **2009**, *93*, 1482–1487. [CrossRef]

22. Sensfuss, S.; Blankenburg, L.; Schache, H.; Shokhovets, S.; Erb, T.; Konkin, A.; Herasimovich, A.; Scheinert, S.; Shahid, M.; Sell, S. Thienopyrazine-based low-bandgap polymers for flexible polymer solar cells. *Eur. Phys. J. Appl. Phys.* **2010**, *51*, 33204–33209. [CrossRef]

23. Soylu, M. GaAs heterojunction devices with MDMO-PPV thin films. *Vacuum* **2014**, *106*, 33–38. [CrossRef]

24. Chen, Y.-H.; Ho, C.-H. Temperature dependence of direct and indirect band gaps of $Bi_{13}I_2S_{18}$ hexagonal rod crystals. *Mater. Chem. Phys.* **2018**, *206*, 71–75. [CrossRef]

25. Urbach, F. The long-wavelength edge of photographic sensitivity and of the electronic absorption of solids. *Phys. Rev.* **1953**, *92*, 1324. [CrossRef]

26. Tommalieh, M.; Zihlif, A. Optical properties of polyimide/silica nanocomposite. *Phys. B Condens. Matter.* **2010**, *405*, 4750–4754. [CrossRef]

27. Pichler, K.; Halliday, D.; Bradley, D.; Burn, P.; Friend, R.; Holmes, A.J. Optical spectroscopy of highly ordered poly (p-phenylene vinylene). *Phys. Condens. Matter.* **1993**, *5*, 7155. [CrossRef]

28. Qaid, S.M.; Al-Asbahi, B.; Ghaithan, H.M.; AlSalhi, M.J. Optical and structural properties of $CsPbBr_3$ perovskite quantum dots/PFO polymer composite thin films. *Colloid Interface Sci.* **2020**, *563*, 426–434. [CrossRef]

29. Zou, J.; Le Rendu, P.; Musa, I.; Yang, S.-H.; Dan, Y.; That, C.T.; Nguyen, T. Investigation of the optical properties of polyfluorene/ZnO nanocomposites. *Thin Solid Films* **2011**, *519*, 3997–4003. [CrossRef]

30. Lee, T.W.; Park, O.O.; Yoon, J.; Kim, J.J. Polymer-layered silicate nanocomposite light-emitting devices. *Adv. Mater.* **2001**, *13*, 211–213. [CrossRef]

31. Yang, S.-H.; Le Rendu, P.; Nguyen, T.P.; Hsu, C.-S. Fabrication of MEH-PPV/SiO_2 and MEH-PPV/TiO_2 nanocomposites with enhanced luminescent stabilities. *Rev. Adv. Mater. Sci.* **2007**, *15*, 144–149.

32. He, G.; Li, Y.; Liu, J.; Yang, Y. Enhanced electroluminescence using polystyrene as a matrix. *Appl. Phys. Lett.* **2002**, *80*, 4247–4249. [CrossRef]

33. Judd, D.B.; MacAdam, D.L.; Wyszecki, G.; Budde, H.; Condit, H.; Henderson, S.; Simonds, J.J. Spectral distribution of typical daylight as a function of correlated color temperature. *Opt. Soc. Am.* **1964**, *54*, 1031–1040. [CrossRef]

34. Carmona-Téllez, S.; Falcony, C.; Aguilar-Frutis, M.; Alarcon-Flores, G.; García-Hipólito, M.; Martínez-Martínez, R. White light emitting transparent double layer stack of Al_2O_3: Eu^{3+}, Tb^{3+}, and Ce^{3+} films deposited by spray pyrolysis. *ECS J. Solid State Sci. Technol.* **2013**, *2*, R111–R115. [CrossRef]